The impact of temperature vertical variability on trajectory modeling of stratospheric water vapour

T. Wang[1,2], A. E. Dessler[1], M. R. Schoeberl[3], W. J. Randel[4], J.-E. Kim[5]

[1]{Texas A&M University, College Station, Texas}

[2]{NASA Jet Propulsion Laboratory/California Institute of Technology, Pasadena, California}

[3]{Science and Technology Corporation, Columbia, Maryland}

[4]{National Center for Atmospheric Research, Boulder, Colorado}

[5]{University of Colorado, Boulder, Colorado}

Correspondence to: Tao Wang (Tao.Wang@jpl.nasa.gov)

Abstract

Lagrangian trajectories driven by reanalysis meteorological fields are frequently used to study water vapour (H_2O) in the stratosphere, in which the tropical cold-point temperatures regulate H_2O amount entering the stratosphere. Therefore, the accuracy of temperatures in the tropical tropopause layer (TTL) is of great importance for understanding stratospheric H_2O abundances. Currently, most reanalyses, such as the NASA MERRA (Modern Era Retrospective-Analysis for Research and Applications), only provide temperatures with ~1.2 km vertical resolution in the TTL, which has been argued misses realistic variability in tropopause temperatures and therefore introduce uncertainties in our understanding of stratospheric H_2O. In this paper, we quantify this uncertainty by comparing the Lagrangian trajectory models using MERRA temperatures on standard model levels (*traj.MER-T*), to those using temperatures with more vertical

variability at the tropopause. This includes GPS temperatures (*traj.GPS-T*) in finer vertical resolution and adjusted MERRA temperatures with enhanced variability induced by underrepresented waves (*traj.MER-Twave*). It turns out that enhanced vertical variability in tropopause temperature more realistically simulates the dehydration of air entering the stratosphere. But the effect on H_2O abundances is relatively minor: comparing with *traj.MER-T, traj.GPS-T* tends to dry air by ~0.1 ppmv while *traj.MER-Twave* tends to dry air by 0.2-0.3 ppmv. Despite these differences in absolute values of predicted H_2O and vertical dehydration patterns, there is virtually no difference in the interannual variability in different runs. Overall, we find that tropopause temperature with finer vertical variability has limited impact on predicted stratospheric H_2O.

1. Introduction

Stratospheric water vapour (H_2O) and its feedback play an important role in regulating the global radiation budget and the climate system (e.g., Holton et al., 1995; Randel et al., 2006; Solomon et al., 2010; Dessler et al., 2013). It has been known since Brewer's seminal work on stratospheric circulation that tropical tropopause temperature is the main driver of stratospheric H_2O concentration (Brewer, 1949). As parcels approach and pass through the cold-point tropopause – the altitude at which air temperature is coldest, condensation occurs and ice falls out, thereby regulating the parcel's H_2O concentration to local saturation level (e.g., Fueglistaler et al., 2009, and references therein). This is the dehydration process. The role of tropopause temperature variation in tropical dehydration is most apparent in the annual variation in tropical stratospheric H_2O, also known as the "tape recorder" (Mote et al., 1996).

When air crosses the tropical tropopause layer (TTL), it experiences multiple dehydrations due to encounter of lower temperatures, and the final stratospheric H_2O mixing ratio is established after air passing through the coldest temperature along its path, which sets the strong relation between cold-point tropopause and the entry level H_2O (e.g., Holton and Gettelman, 2001; Randel et al., 2004, 2006).

The details of the transport and dehydration process can be understood by performing Lagrangian trajectory simulations, which track the temperature history of a large number of individual parcels. Unlike simulation of chemical tracers that depends strongly on the transport imposed (Ploeger et al., 2011; Wang et al., 2014), the simulation of H_2O is primarily constrained by tropopause temperatures. Dehydration thus primarily depends on the air parcel temperature history, and stratospheric H_2O simulations ultimately require accurate analyses of temperatures particularly in the tropopause (e.g., Mote et al., 1996; Fueglistaler et al., 2005, 2009; Liu et al., 2010; Schoeberl and Dessler, 2011; Schoeberl et al., 2012, 2013).

In this paper, we use a forward, domain-filling trajectory model to study the detailed dehydration behavior of the humidity of air parcels entering the tropical lower stratosphere. Previous analyses have demonstrated that this model can accurately simulate many of the aspects of the observed stratospheric H_2O (Schoeberl and Dessler, 2011; Schoeberl et al., 2012, 2013). Despite the good agreements with observations, there are clear areas of uncertainty, such as the accuracy of circulation fields (Schoeberl et al., 2012), the details of the dehydration mechanisms (Schoeberl et al., 2014), the influences

from convection (Schoeberl et al., 2011, 2014), and the impacts of unresolved temperature variability in the TTL, etc. In this paper, we investigate uncertainties introduced by the last one – the effect of vertical variability of temperatures.

This is accomplished by comparing trajectory results from using NASA Modern Era Retrospective-Analysis for Research and Applications (MERRA) (Rienecker et al., 2011) temperatures at standard model levels, to using temperatures with finer vertical variability, which include GPS temperatures and the MERRA temperatures adjusted to account for resolved but underrepresented waves (Kim and Alexander, 2013). This will help us to further understand the importance of tropopause temperature variability in dehydrating air entering the stratosphere.

2. Trajectory Model and Temperatures Used

2.1 Trajectory model

The trajectory model used here follows the details described in Schoeberl and Dessler (2011) with parcel positions integrated using the Bowman trajectory code (Bowman, 1993; Bowman et al., 2013). This model has been proven capable of simulating stratosphere H_2O and its long-term variability (Schoeberl and Dessler, 2011; Schoeberl et al., 2012, 2013; Dessler et al, 2014), modeling chemical tracers transport in the lower stratosphere (Wang et al., 2014), and studying the stratosphere air age spectrum (Ray et al., 2014). Because of the overly dispersive behavior of kinematic trajectories (e.g., Schoeberl et al., 2003; Liu et al., 2010; Ploeger et al., 2010; Schoeberl and Dessler, 2011), we perform diabatic trajectories using isentropic coordinates, in which the vertical

velocity is the potential temperature tendency converted from the diabatic heating rates via the thermodynamic equation (e.g., Andrews et al., 1987). Here we used total heating rates, which include heating due to long-wave and short-wave radiation, moist physics, friction, etc.

The parcel initiation level is chosen to be the 370-K isentrope, which is above the level of zero radiative heating (~355-365 K, Gettelman and Forster, 2002) and below the tropical tropopause (~375–380 K) in the tropics. Every day, parcels are initialized on equal area grids covering 40^{o}N–40^{o}S and advected forward in time by reanalysis winds. At the end of each day, any parcels that have descended below the 345 K (~250 hPa or ~10 km) level are removed since in most cases they have entered the troposphere. The upper boundary is chosen to be 2200 K isentrope (~1 hPa or ~50 km) to cover the entire stratosphere. Parcels are initialized and added to the ensemble consecutively on every day and the combined set of parcels is then advected forward. This process is repeated over the entire integration period so that after 2-3 years the stratospheric domain is filled up with parcels – this is the concept of domain-filling, which guarantees a robust statistics.

H_2O is conserved along the trajectories, except when saturation occurs; in that case, excess H_2O is instantaneously removed from the parcel to keep the relative humidity with respect to ice from exceeding 100%. This is sometimes referred as “instant dehydration” (e.g., Schoeberl et al., 2014), which ignores detailed microphysics but has shown to simulate many features of H_2O in the lower stratosphere (e.g., Fueglistaler et al., 2005; Jensen and Pfister, 2004; Gettelman et al., 2002). We chose the 100% saturation level

because 1) different saturation levels offset the simulated H_2O constant values but with identical interannual variability; and 2) the focus of the paper is to investigate the uncertainty introduced by using different temperatures, which would be the same as long as we keep the same criteria for different runs.

In addition to H_2O, we also carry methane (CH_4) concentration for each parcel. We initiate CH_4 values increased from 1.76 ppmv in 2006 to 1.83 ppmv in 2013. As described in Schoeberl and Dessler (2011), we use photochemical loss rates supplied from Goddard two-dimensional stratospheric chemistry model (Fleming et al., 2007) to convert each methane molecule into two molecules of H_2O (Dessler et al., 1994). Noted that our analysis focus on the tropical lower stratosphere, where methane oxidation has little impacts on the total H_2O abundances (Fig. 6 in Schoeberl et al., 2012).

Along each trajectory, we locate the point when air experiences coldest temperature as the final dehydration point (FDP), which determines the stratosphere entry level H_2O mixing ratio (FDP-H_2O) for that trajectory. As will be shown below, the entry level H_2O predicted by the trajectory model is affected by the vertical variability in temperature field.

2.2 Temperature datasets

In this paper, we use MERRA (Rienecker et al., 2011) circulation to advect parcels. This includes horizontal wind components and total diabatic heating rates. As shown in Schoeberl et al. (2012, 2013), trajectory model driven by this reanalysis yields excellent

140 estimates of H_2O compared to observations by the Aura Microwave Limb Sounder
141 (MLS) (Read et al., 2007).
142
143 Driven by the same circulation, we use three different temperature datasets to quantify
144 the uncertainty induced by temperatures with different variability in the vertical: 1)
145 MERRA standard temperatures on model levels (MER-T), denoted as *traj.MER-T*; 2)
146 GPS radio occultation (RO) temperatures, denoted as *traj.GPS-T*; and 3) MERRA
147 temperatures enhanced by wave scheme to recover the variability not represented well in
148 current coarse model levels (Kim and Alexander, 2013), denoted as *traj.MER-Twave*.
149 Note that MERRA does not assimilate GPS observations, which makes the two
150 temperature datasets independent from each other. Trajectory runs with the three different
151 temperature datasets are summarized in Table 1.
152
153 **2.2.1 GPS temperature**
154 Owing to its high vertical resolution, GPS temperature profiles capture the cold-point
155 tropopause with high accuracy. In this paper we use GPS wet profile (wetPrf) retrieved at
156 100-m vertical resolution using a one-dimensional variational technique based on
157 ECMWF analysis. The wetPrf and GPS Atmospheric Profile (atmPrf, derived assuming
158 no water vapor in the air) temperatures are essentially the same in 200-10 hPa but below
159 200 hPa the errors in atmPrf could be as high as ~ 3 K due to neglect of water vapour
160 (Das and Pan, 2014). Despite being retrieved at 100-m resolution, the actual vertical
161 resolution ranges from 0.5 km in the lower troposphere to ~1 km in the middle
162 atmosphere (Kursinski et al., 1997).

163

164 The GPS radio occultation (RO) technique makes the data accuracy independent of
165 platforms. That makes the biases among different RO payloads could be as low as 0.2 K
166 in the tropopause and stratosphere (Ho et al., 2009). Therefore, to compensate the
167 relatively lower horizontal resolution (relative to that of reanalysis), we include GPS RO
168 from all platforms. This include the Constellation Observing System for Meteorology,
169 Ionosphere, and Climate (COSMIC) (Anthes et al., 2008), the CHAllenging Minisatellite
170 Payload (CHAMP) satellite (Wickert et al., 2001), the Communications/Navigation
171 Outage Forecasting System (CNOFS), the Gravity Recovery And Climate Experiment
172 (GRACE) twin satellites (Beyerle et al., 2005), the Meteorological Operational Polar
173 Satellite–A (MetOp-A), the Satellite de Aplicaciones Cientifico-C (SACC) satellite (Hajj
174 et al., 2004), and the TerraSAR-X (TerraSAR-X). There are ~2000-3500 profiles per day,
175 mostly from COSMIC, with ~800-1100 profiles of these in the tropics.

176

177 Each day, GPS temperature profiles are binned to 200-m vertical resolution. Horizontally,
178 we grid data into 2.5x1.25 (longitude by latitude) grids with 2-D Gaussian function
179 weighting. This gridded dataset has been successfully used in diagnosing many detailed
180 features of tropopause inversion layer (Gettelman and Wang, 2015). We use over 7 years
181 of GPS data available from July 2006 to December 2013, and the trajectory run using it is
182 denoted as *traj.GPS-T*.

183

184 Fig. 1 shows a snapshot of the 100-hPa GPS raw (panel a) and gridded (panel b)
185 temperature on January 1st, 2010, compared with MERRA temperature (panel c). It

186 demonstrates that the gridded GPS temperature captures most of the variability, although
187 some detailed structure might be lost due to its relatively sparse sampling.
188
189 Fig. 2 shows the GPS and MERRA temperatures in the TTL (panel a) and their
190 differences (GPS–MERRA) (panel b, extended to 31 hPa) averaged over the deep tropics
191 (18^{o}S–18^{o}N) during the GPS period. Here, we examine the values at the MERRA model
192 levels (larger dots) as well as MERRA in-between levels (smaller dots), where both GPS
193 and MERRA temperatures are linearly interpolated to the same pressure levels. It shows
194 that the GPS is at most ~0.4 K colder than MERRA around the cold-point tropopause
195 (~93 hPa on average, in-between MERRA coarse levels), where temperature is ~193 K.
196 This translates to at most a 0.4 ppmv wet bias in the entry level of stratospheric H_2O,
197 assuming 100% saturation level. Note that the GPS temperatures at MERRA levels 100
198 and 85 hPa could be lower than that in MERRA if we average over 10^{o}S–10^{o}N, but it
199 does not change the fact that MERRA is always warm biased around the cold-point
200 tropopause.
201
202 **2.2.2 MERRA temperature adjusted by waves**
203 Wave-induced disturbances on tropopause temperatures are underrepresented by current
204 reanalyses (Kim and Alexander, 2013). At the reanalysis model levels, temperature
205 variability at time scales shorter than ~10 days are weaker than radiosondes observations
206 (refer Fig. 1b-d in Kim and Alexander, 2013). Those underrepresented waves include a
207 part of the spectrum of Kelvin waves, mixed Rossby-gravity waves, and gravity waves.
208 Moreover, when used in trajectory simulations, conventional interpolation of model level

temperatures to in-between levels, either linear or higher order, degrades temperature variability even at longer time scales (> 10 days). This is because observed temperature profiles have strong curvatures in-between coarse model levels due to the existence of fine vertical-scale waves.

To overcome these limitations, a scheme developed by Kim and Alexander, based on amplitude-phase interpolation and wave amplification from radiosonde observations, has been proven to be effective in recovering the underrepresented variability in reanalysis temperatures (refer Kim and Alexander, 2013 for more details). Applying this scheme on MERRA temperature records yields a new MERRA temperature dataset (MER-Twave) that has more realistic temperature variability induced by waves (refer Fig. 3 in Kim and Alexander, 2013). The trajectory simulation using this temperature dataset is denoted as *traj.MER-Twave*.

Note that we only considered the vertical resolution issue, since it is by far a limiting factor in representing waves in the TTL. A large portion of a TTL wave spectrum has horizontal and temporal scales much larger and longer than reanalysis resolution, therefore, temperature behaves almost linearly in-between model horizontal and temporal resolution. However, temperature does not behave linearly in vertical space due to the fact that a significant portion of TTL waves have vertical wavelengths shorter than ~4 km (see Figure S4 in supporting information of Kim and Alexander, 2015), which could make waves less represented by the ~1.2 km vertical resolution in reanalyses.

The wave scheme produces both positive and negative perturbations to the MERRA temperature profiles, depending on the phase of waves. Overall, the change in temperature induced by waves is less than 2 K (Fig. 3), although in rare cases it can reach 5-7 K. Importantly, however, about 80% of the changes in cold-point temperature are negative, with the wave scheme lowering the average cold-point temperatures by ~0.35 K. It is this reduction in cold-point temperature that is responsible for the reduction in H_2O entering the stratosphere.

Note that we included both GPS and MER-Twave datasets because they have their own advantages and limitations. GPS provides sparse sampling in the tropics (only ~800-1100 profiles per day), indicating a smaller horizontal variability in GPS than likely exists, but the mean temperatures are more accurate. In contrast, MER-Twave has better variability but not accurate mean, since it is designed to have similar temperature variability to radiosondes but with mean reserved to original MER-T. In summary, the mean temperature is closer to reality in GPS than in MER-T and MER-Twave, but the temperature variability is closer to reality in MER-Twave than in MER-T and GPS. In addition, the MER-Twave is a general technique that could be applied to situations where GPS temperatures are not available (e.g., reanalyses before 2006, climate models).

2.2.3 Interpolation scheme

In our studies, we use linear interpolation to estimate the temperature between the fixed levels of temperature data sets. However, some previous analyses have used higher order interpolations, such as cubic spline (e.g., Liu et al., 2010), to make assumptions about the

255 strong curvature of temperature profiles around the cold-point tropopause. In order to
256 determine which approach is superior, we sample GPS tropical temperature profiles at
257 MERRA vertical levels and then use the two interpolation schemes to reconstruct the full
258 GPS resolution. Then we compare the minimum saturation mixing ratio from the
259 recovered profiles to the minimum calculated from the full resolution GPS profiles.
260
261 Fig. 4a shows the probability distribution of the differences between the minimum
262 saturation mixing ratio in the full-resolution GPS profile and in the two interpolation
263 schemes. On average, the linear interpolation performs better (RMS difference is 0.18
264 and 0.25 ppmv for the linear and cubic spline, respectively). Fig. 4b shows the
265 corresponding probability distribution of the difference of the pressure of this minimum,
266 and the linear interpolation does better for this metric, too (RMS difference is 5.2 and 7.2
267 hPa for the linear and the cubic spline interpolation, respectively). We have also tested
268 higher order spline interpolations and find that none produce lower RMS errors than
269 linear interpolation. Overall, cubic spline interpolation tends to underestimate cold-point
270 temperature, making the implied H_2O too dry, as noted by Liu et al., (2010). Thus, in our
271 studies we adopted linear interpolation scheme for three different trajectory integrations.
272

273 ## 3. Trajectory Results

274 ### 3.1 Dehydration patterns

275 The gridded GPS temperatures are available since July 2006, so for fair comparison we
276 start all trajectory runs at that time and run them forward till the end of 2013. For each
277 model run, we calculate statistics of the final dehydration points (FDP) for all parcels
278 entering the stratosphere. We define "parcels entering the stratosphere" as parcels that

underwent final dehydration between 45°N–45°S (thus ignoring polar dehydration) and that were already at altitudes higher (pressure lower) than 90 hPa for at least six months since the last time they were dehydrated (FDP). This guarantees that parcels already crossed the cold-point tropopause (~380 K or ~100-94 hPa) and has indeed experienced the coldest temperature along its ascending paths. Averaging over 7 years minimizes the effects of interannual variability.

Fig. 5a-c compares the FDP frequency (solid lines) and the FDP H_2O (dashed lines) in different seasons among three runs. As mentioned, the FDP H_2O can be understood as the stratosphere entry level of H_2O. In all cases, it is clear that dehydration occurs almost exclusively between 60 and 110 hPa. The average FDP H_2O reaches a minimum at 85 hPa for all runs, meaning parcels dehydrated in its vicinity carry the smallest amount of H_2O into the stratosphere. The relatively high FDP-H_2O above 80 hPa (just above the entry level) comes from the parcels that avoided the tropical cold trap and experienced final dehydration at higher, warmer levels of the stratosphere. Out of ~1.3 millions of parcels in the stratosphere there are only ~0.3% bypassed the cold-point tropopause, and these parcels have little impact on the stratosphere water vapour.

The FDP frequency, however, shows large differences among three runs. The run using MERRA temperature (*traj.MER-T*) yields an annual bimodal FDP maxima distinctly at 98 and 84 hPa (Fig. 5a solid black lines), close to the MERRA model levels 100.5 and 85.4 hPa, respectively. The bimodal feature comes from averages between single, prominent peaks during DJF (December-January-February, Fig. 5a, blue) and JJA (June-

July-August, Fig. 5a, red), when cold-point tropopause is close to a particular level (DJF to 85 hPa and JJA to 100 hPa) in MERRA (Fig. 5d-e black bars), as well as averages between bi-modal peaks during MAM (March-April-May, Fig. 5a, green) and SON (September-October-November, Fig. 5a, yellow), when tropopause temperature in real atmosphere fall in between the two MERRA levels (Fig. 5f red bars). The dehydration profiles implied from using the other two datasets, however, experience smoothed changes due to gradual variations of cold-point altitudes in each season (red and blue bars in Fig. 5d-f). It is clear that more realistic dehydrations (Fig. 5b-c) occur with more variability in tropopause temperature (Fig. 5d-f red and blue bars).

Note that at FDP, the coldest temperature encountered could be either at MERRA model levels or in-between levels during that step of integration, depending on the trajectory integration intervals. Suppose our trajectory integration time step is as small as seconds, then at some time steps parcels would inevitably travel to each of the MERRA model levels, and therefore the encountered coldest temperatures would always be at either of the two levels in MERRA. In another word, the bimodal FDP distribution from MERRA run (Fig. 5a) could be even more peaked when choosing smaller integration step. Two reasons that we didn't choose such small time step: 1) the wind and temperature data are only available 6-hourly or even daily (GPS) so much smaller time step introduces more uncertainties with more interpolation; and 2) considering the balance between model running speed and computational resources.

Fig. 6 depicts the vertical distributions of normalized FDP in time (panel a-c) and

longitude (panel d-f) sectors for the three different runs. We see that the MERRA coarse model levels do not capture the variations of cold-point tropopause well during MAM and SON, resulting in discontinuous transition of FDP from DJF to MAM, and from JJA to SON (panel a). When using GPS temperatures (panel b) and MERRA temperatures adjusted to recover wave-induced variability (panel c), the dehydration patterns show continuous variations throughout the year. The bimodal feature is more emphasized in the longitudinal-vertical view (panel d), where we can also see that throughout a year the most frequent dehydrations occur over the western tropical pacific region.

3.2 Water Vapour (H_2O)

It is obvious that trajectory simulations using GPS temperatures (*traj.GPS-T*) and MERRA temperatures adjusted by waves (*traj.MER-Twave*) tend to yield more reasonable FDP patterns around the cold-point tropopause (Fig. 5 solid lines), although the parcels dehydrated at particular altitudes have similar amounts of H_2O in all three models (FDP H_2O, Fig. 5 dashed lines). A more interesting question is whether the different dehydration occurrences affect the stratospheric H_2O predicted by the trajectory model.

Fig. 7a shows the tropical (18°N–18^{o}S) H_2O profile predicted from three trajectory runs compared with MLS observations. The vertical bars in MLS indicate the MLS vertical resolutions at each of the MLS retrieval pressure levels. Here, we see clearly that the H_2O in stratosphere reflects the different cold-point temperatures in three datasets. The differences induced more variability in temperatures are clearly shown in Fig. 7b, where we see slightly drier air expected in GPS run since GPS temperatures are at most ~0.4 K

lower than that of MERRA around the tropopause (Fig. 2); whereas enhanced wave perturbations produce air 0.2-0.3 ppmv drier, in agreement with previous calculations (e.g., Jensen et al., 2004; Schoeberl et al., 2011).

Fig. 8c also shows that comparing to *traj.MER-T*, the dry biases from using GPS temperatures are largest in MAM and SON (0.14-0.21 ppmv on average), when the real cold-point tropopause cannot be resolved by the MERRA model levels. During DJF and JJA, when the cold point is near one of the two MERRA standard levels, the differences become smaller. Thus we conclude that using GPS temperatures decreases simulated stratospheric H_2O by an average of ~0.1 ppmv, accounting for ~2.5% given typical stratospheric H_2O abundances of ~4 ppmv.

It is important to point out that, despite these differences in the absolute value of H_2O, there is virtually no difference in the anomalies (remainder from the average annual cycle). In Fig. 8a we compare the time series of H_2O anomalies at 83 hPa from the three different trajectory runs weighted by the MLS averaging kernels as well the MLS observations. Note that the interannual variations of approximately ±0.5 ppmv in H_2O are in good agreement with the interannual changes of about ±1 K in cold-point tropopause temperatures (Fig. 8b) for all three different runs, further supporting that the stratospheric entry level of H_2O and cold-point tropopause temperature are strongly coupled (e.g., Randel et al., 2004, 2006; Randel and Jensen, 2013). We also compared *traj.MER-T* and *traj.MER-Twave* over longer period (1985-2013) and it shows almost no differences in interannual variability, either. Clearly, for studying the interannual variability of H_2O,

372 MERRA temperatures in coarse vertical resolution are as good as temperatures in higher
373 vertical resolution.
374
375 **4. Summary**
376 The dehydration of air entering the stratosphere largely depends on the cold-point
377 temperature around the tropopause. This may not be represented accurately by reanalyses
378 due to the relatively coarse vertical resolution with less variability in cold-point
379 tropopause temperatures. To investigate the impacts of this, we compare trajectory results
380 from using standard MERRA model level temperatures to those using temperature
381 datasets in finer vertical resolution with enhanced variability. This includes GPS
382 temperatures and adjusted MERRA temperatures with enhanced vertical variability
383 induced by wave scheme developed by Kim and Alexander (2013).
384
385 Compared with the standard MERRA temperatures, we find that using higher resolution
386 GPS temperatures dries the H_2O prediction by ~0.1 ppmv, and using MERRA
387 temperatures adjusted by wave scheme dries the stratosphere by ~0.2-0.3 ppmv (Fig. 7a-
388 b). This is consistent with previous analyses (e.g., Jensen et al., 2004; Schoeberl et al.,
389 2011). Despite the small differences in H_2O abundances, the interannual variability
390 (residual from the mean annual cycle) exhibits virtually no differences, due to the strong
391 coupling between stratospheric H_2O and tropical cold-point temperatures (Fig. 8).
392 Therefore, in terms of studying the interannual changes of stratospheric H_2O, we argue
393 that reanalysis temperatures are more useful due to its long-term availability.
394

Looking at the locations of FDP, we find a bimodal distribution when using standard MERRA temperatures on model levels (Figs. 5-6). This is caused by the fact that the cold-point tropopause is constrained to be near the two MERRA model levels (100.5 and 85.4 hPa) that bracket the cold-point tropopause (Fig. 5d-f, black histograms). When using the temperatures in higher vertical resolution with more variability, the resultant FDP patterns appear to be more physically reasonable (Figs. 5-6),

In this paper we perform linear interpolations for all trajectory runs. Other analyses have used cubic spline interpolation owing to the strong curvature of temperature profile around the cold-point tropopause. We investigate the performances of both schemes using GPS temperature profiles (Sect. 2.2.3) and find that while introducing new information due to its assumption in the temperature profile around the tropopause, cubic spline scheme tends to generate unrealistically low cold-point temperature due to cubic fitting. Therefore, the results are not necessarily realistic and on the other hand linear interpolation is overall more accurate (Fig. 4).

It is well known that TTL temperatures regulate stratospheric humidity. In this paper, we have investigated one issue in our understanding of TTL temperatures — the effect of finer vertical resolution that may have captured more variability in tropopause temperatures — and find that it is comparatively minor. This provides some confidence that the trajectory model driven by current modern reanalyses is capable of depicting the stratospheric water vapour accurately.

Acknowledgements

The authors thank Kenneth Bowman, Joan Alexander, and Eric Jensen for their helpful discussions and comments. This work was supported by NSF AGS-1261948, NASA grant NNX13AK25G and NNX14AF15G, and partially under the NASA Aura Science Program. This work was partially carried out during visits of Tao Wang funded by the Graduate Student Visitor Program under the Advanced Study Program (ASP) at the National Center for Atmospheric Research (NCAR), which is operated by the University Corporation for Atmospheric Research, under sponsorship of the National Science Foundation.

References

Andrews, D. G., Holton, J. R., and Leovy, C. B.: Middle Atmosphere Dynamics, Academic Press, Orlando, Florida, 489 pp, 1987.

Anthes, R. A., et al.: The COSMIC/FORMOSAT‑3 mission: Early results, Bull. Am. Meteorol. Soc., 89, 313–333, doi:10.1175/BAMS-89- 3-313, 2008.

Beyerle, G., Schmidt, T., Michalak, G., Heise, S., Wickert, J., and Reigber, Ch.: GPS radio occultation with GRACE: Atmospheric profiling utilizing the zero difference technique, Geophys. Res. Lett., 32, L13806, doi:10.1029/2005GL023109, 2005.

Bowman, K. P.: Large-scale isentropic mixing properties of the Antarctic polar vortex from analyzed winds, J. Geophys. Res., 98, 23013–23027, 1993.

Bowman, K. P., Lin, J. C., Stohl, A., Draxler, R., Konopka, P., Andrews, A., and Brunner, D.: Input data requirements Lagrangian Trajectory Models, B. Am. Meteorol. Soc., 94, 1051– 1058, doi:10.1175/BAMS-D-12-00076.1, 2013.

Brewer, A. W.: Evidence for a world circulation provided by the measurements of helium and water vapor distribution in the stratosphere, Q. J. R. Meteorol. Soc., 75, 351–363, 1949.

Das, U. and Pan, C. J.: Validation of FORMOSAT-3/COSMIC level 2 "atmPrf" global temperature data in the stratosphere, Atmos. Meas. Tech., 7, 731-742, doi:10.5194/amt-7-731-2014, 2014.

Dessler, A. E., Weinstock, E. M., Hintsa, E. J., Anderson, J. G., Webster, C. R., May, R. D., Elkins, J. W., and Dutton, G. S.: An examination of the total hydrogen budget of the lower stratosphere, Geophys. Res. Lett., 21, 2563–2566, 1994.

Dessler, A. E., Schoeberl, M. R., Wang, T., Davis, S. M., and Rosenlof, K. H.: Stratospheric water vapor feedback, P. Natl. Acad. Sci. USA, 110, 18087–18091, doi:10.1073/pnas.1310344110, 2013.

Dessler, A. E., Schoeberl, M. R., Wang, T., Davis, S. M., and Rosenlof, K. H., Vernier, J.-P.: Variations of Stratospheric Water Vapor Over the Past Three Decades, J. Geophys. Res. 119, DOI: 10.1002/2014JD021712, 2014.

Fleming, E. L., Jackman, C. H., Weisenstein, D. K., and Ko, M. K. W.: The impact of interannual variability on multidecadal total ozone simulations, J. Geophys. Res., 112, D10310, doi:10.1029/2006JD007953, 2007.

Fueglistaler, S., Bonazzola, M., Haynes, P. H., and Peter, T.: Stratospheric water vapor predicted from the Lagrangian temperature history of air entering the stratosphere in the tropics, J. Geophys. Res., 110, D08107, doi:10.1029/2004JD005516, 2005.

Fueglistaler, S., Dessler, A. E., Dunkerton, T. J., Folkins, I., Fu, Q., and Mote, P. W.: The tropical tropopause layer, Rev. Geophys., 47, RG1004, doi:10.1029/2008RG000267, 2009.

Gettelman, A. and Forster, P. M. de: Definition and climatology of the tropical tropopause layer, Journal of the Meteorological Society of Japan, 80:4B, 911-924, 2002.

Gettelman, A., Randel, W. J., Wu, F., and Massie, S. T.: Transport of water vapor in the tropical tropopause layer, Geophys. Res. Lett., edited, p. 10.1029/2001GL013818, 2002.

Gettelman, A., and Wang, T.: Structural diagnostics of the tropopause inversion layer and its evolution, J. Geophys. Res. Atmos., 120, doi:10.1002/2014JD021846, 2015.

Hajj, G. A., Ao, C. O., Iijima, B. A., Kuang, D., Kursinski, E.R., Mannucci, A. J.,

Meehan, T. K., Romans, L. J., de La Torre Juarez, M., and Yunck, T. P.: CHAMP and SAC-C atmospheric occultation results and intercomparisons, J. Geophys. Res., 109, D06109, doi:10.1029/2003JD003909, 2004.
Ho, S.-P., Goldberg, M., Kuo, Y.-H., Zou, C.-Z., and Schreiner, W.: Calibration of temperature in the lower stratosphere from microwave measurements using COSMIC radio occultation data: Preliminary results, Terr. Atmos. Ocean. Sci., 20, 87–100, 2009.
Holton, J. R., Haynes, P. H., McIntyre, M. E., Douglass, A. R., Rood, R. B., Pfister, L.: Stratosphere-troposphere exchange, Rev. Geophys., 334, 405–439, 1995.
Holton, J. R., and Gettelman, A.: Horizontal transport and the dehydration of the stratosphere, Geophys. Res. Lett., 28(14), 2799–2802, doi:10.1029/2001GL013148, 2001.
Jensen, E., and Pfister, L.: Transport and freeze-drying in the tropical tropopause layer, J. Geophys. Res., 109, D02207, doi:10.1029/2003JD004022, 2004.
Kim, J.-E., and Alexander, J. M.,: A new wave scheme for trajectory simulations of stratospheric water vapor, Geophys. Res. Lett., 40, 5286–5290, doi:10.1002/grl.50963, 2013.
Kim, J.-E., and Alexander, J. M.,: Direct impacts of waves on tropical cold point tropopause temperature, Geophys. Res. Lett., doi:10.1002/2014GL062737, 2015.
Kursinski, E. R., Hajj, G. A., Schofield, J. T., Linfield, R. P., and Hardy, K. R.: Observing Earth's atmosphere with radio occultation measurements using the Global Positioning System, J. Geophys. Res., 102(D19), 23429–23465, doi:10.1029/97JD01569, 1997.
Liu, Y. S., Fueglistaler, S., and Haynes, P. H.: Advection-condensation paradigm for stratospheric water vapor, J. Geophys. Res., 115, D24307, doi:10.1029/2010jd014352, 2010.
Mote, P. W., Rosenlof, K. H., McIntyre, M. E., Carr, E. S., Gille, J. C., Holton, J. R., Kinnersley, J. S., Pumphrey, H. C., Russell III, J. M., and Waters, J. W.: An atmospheric tape recorder: the imprint of tropical tropopause temperatures on stratospheric water vapor, J. Geophys. Res., 101, 3989–4006, 1996.
Ploeger, F., Konopka, P., Gu¨nther, G., Grooß, J.-U., and Mu¨ller, R.: Impact of the vertical velocity scheme on modeling transport across the tropical tropopause layer, J. Geophys. Res., 115, doi:10.1029/2009JD012023, 2010.
Ploeger, F., Fueglistaler, S., Grooß, J.-U., Gu¨nther, G., Konopka, P., Liu, Y. S., Mu¨ller, R., Ravegnani, F., Schiller, C., Ulanovski, A., and Riese, M.: Insight from ozone and water vapour on transport in the trop- ical tropopause layer (TTL), Atmos. Chem. Phys., 11, 407–419, doi: 10.5194/acp-11-407-2011, 2011.
Randel, W. J., Wu, F., Oltmans, S. J., Rosenlof, K. H., Nedoluha, G. E.,: Interannual Changes of Stratospheric Water Vapor and Correlations with Tropical Tropopause Temperatures. J. Atmos. Sci., 61, 2133–2148. doi: http://dx.doi.org/10.1175/1520-0469(2004)061<2133:ICOSWV>2.0.CO;2, 2004.
Randel, W. J., Wu, F., Vömel, H., Nedoluha, G. E., and Forster, P.: Decreases in stratospheric water vapor after 2001: Links to changes in the tropical tropopause and the Brewer-Dobson circulation, J. Geophys. Res., 111, D12312, doi:10.1029/2005JD006744, 2006.
Randel, W. J. and Jensen, E. J.: Physical processes in the tropical tropopause layer and

519 their role in a changing climate, Nat. Geosci., 6, 169–176, doi:10.1038/ngeo1733,
520 2013.
521 Ray, E.A., Moore, F.L, Rosenlof, K.H, Davis, S.M., Sweeney, C., Tans, P., Wang, T.,
522 Elkins, J.W., Bönisch, H., Engel, A., Sugawara, S., T. Nakazawa and S. Aoki:
523 Improving stratospheric transport trend analysis based on SF6 and CO2
524 measurements, J. Geophys. Res. doi: 10.1002/2014JD021802, 2014.
525 Read, W. G., et al.: Aura Microwave Limb Sounder upper tropospheric and lower
526 stratospheric H2O and relative humidity with respect to ice validation, J. Geophys.
527 Res., 112, D24S35, doi:10.1029/2007JD008752, 2007.
528 Rienecker, M. M., Suarez, M. J., Gelaro, R., Todling, R., Bacmeister, J., Liu, E.,
529 Bosilovich, M. G., Schubert, S.D., Takacs, L., Kim, G.-K., Bloom, S., Chen, J.,
530 Collins, D., Conaty, A., da Silva, A., Gu, W., Joiner, J., Koster, R. D., Lucchesi, R.,
531 Molod, A., Owens, T., Pawson, S., Pegion, P., Redder, C. R., Reichle, R., Robertson,
532 F. R., Ruddick, A. G., Sienkiewicz, M., and Woollen, J.: MERRA – NASA's modern-
533 era retrospective analysis for research and applications, J. Climate, 24, 3624–3648,
534 doi:10.1175/JCLI-D-11-00015.1, 2011.
535 Schoeberl, M. R., Douglass, A. R., Zhu, Z. X., and Pawson, S.: A comparison of the
536 lower stratospheric age spectra derived from a general circulation model and two
537 data assimilation systems, J. Geophys. Res., 108, 4113, 2003.
538 Schoeberl, M. R. and Dessler, A. E.: Dehydration of the stratosphere, Atmos. Chem.
539 Phys., 11, 8433–8446, doi:10.5194/acp-11-8433-2011, 2011.
540 Schoeberl, M. R., Dessler, A. E., and Wang, T.: Simulation of stratospheric water vapor
541 and trends using three reanalyses, Atmos. Chem. Phys., 12, 6475–6487,
542 doi:10.5194/acp-12- 6475-2012, 2012.
543 Schoeberl, M. R., Dessler, A. E., and Wang, T.: Modeling upper tropospheric and lower
544 stratospheric water vapor anomalies, Atmos. Chem. Phys., 13, 7783–7793,
545 doi:10.5194/acp-13- 7783-2013, 2013.
546 Schoeberl, M. R., Dessler, A. E., Wang, T., Avery, M. A, Jensen, E.: Cloud Formation,
547 Convection, and Stratospheric Dehydration, Earth and Space Science, DOI:
548 10.1002/2014EA000014, 2014.
549 Solomon, S., Rosenlof, K. H., Portmann, R. W., Daniel, J. S., Davis, S. M., Sanford, T. J.,
550 and Plattner, G.-K.: Contributions of stratospheric water vapor to decadal changes in
551 the rate of global warming, Science, 327, 1219–1223, 2010.
552 Wang, T., Randel, W. J., Dessler, A. E., Schoeberl, M. R., and Kinnison, D. E.: Trajectory
553 model simulations of ozone (O_3) and carbon monoxide (CO) in the lower
554 stratosphere, Atmos. Chem. Phys., 14, 7135-7147, doi:10.5194/acp-14-7135-2014,
555 2014.
556 Wickert, J., Reigber, C., Beyerle, G., Ko¨nig, R., Marquardt, C., Schmidt, T., Grundwaldt,
557 L., Galas, R., Meehan, T. K., Mel- bourne, W. G., and Hocke, K.: Atmosphere
558 sounding by GPS ra- dio occultation: First results from CHAMP: Geophys. Res.
559 Lett., 28, 3263–3266, 2011.

560 **Table**

561

562 **Table 1.** Different temperature datasets used in trajectory model.

Temperature Datasets	Availability	Horizontal Resolution (Longitude x Latitude)	Vertical Resolution In TTL	Trajectory Runs Denoted
MERRA	Daily*	2/3 x 1/2	~1.2 km	*traj.MER-T*
GPS (gridded)	Daily	2.5 x 1.25	0.2 km	*traj.GPS-T*
MERRA w/ waves	Daily*	2/3 x 1/2	0.2 km	*traj.MER-Twave*

563 *These datasets are available 6-hourly. But for fair comparison with using GPS data,
564 we used daily averages.

565 **Figures**

566

567

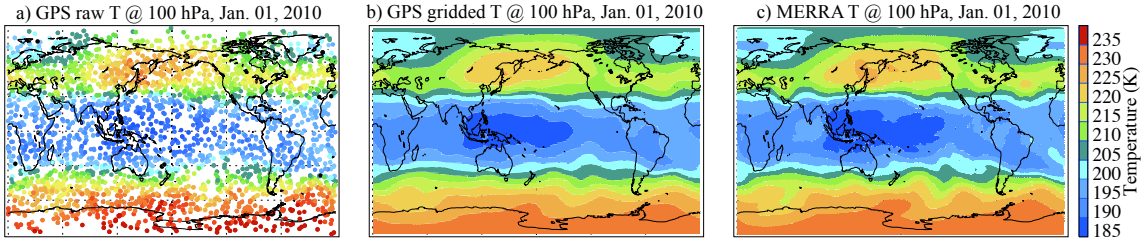

Fig. 1. (a) Comparison of temperatures from raw GPS (panel a), gridded GPS (panel b), and MERRA temperature (panel c) at 100 hPa on Jan. 1st, 2010.

568

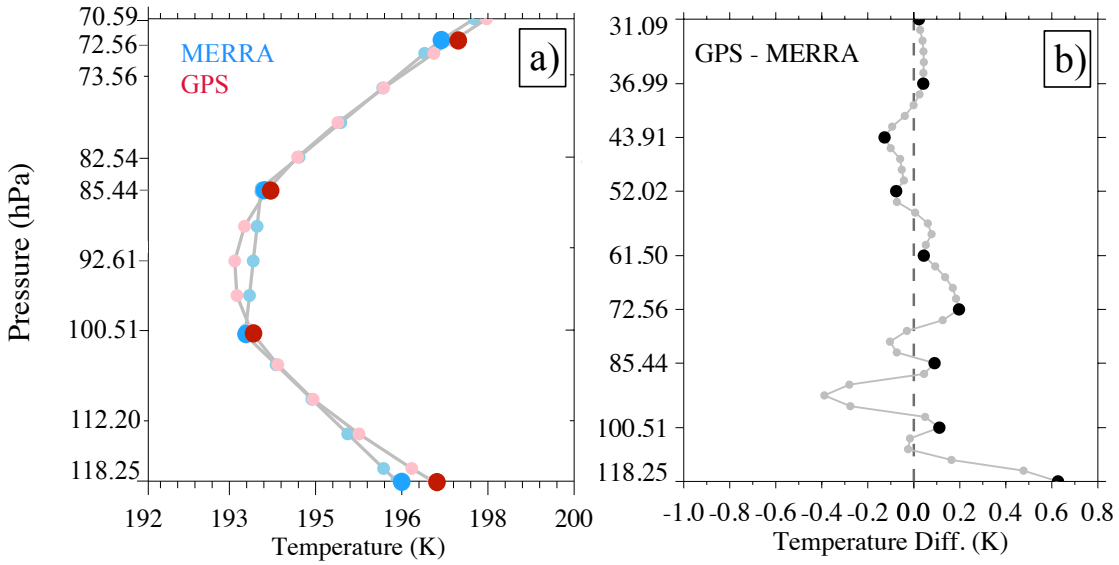

Fig. 2. (a) MERRA (blue) and GPS (red) mean temperature in TTL and (b) their differences (GPS – MERRA) extended to 31 hPa. All values are averaged over the deep tropics (18°S–18°N) in 2007-2013, with larger dots marking the MERRA model levels and small dots marking the MERRA in-between levels, where both GPS and MERRA temperatures are linearly interpolated to the same pressure levels.

569

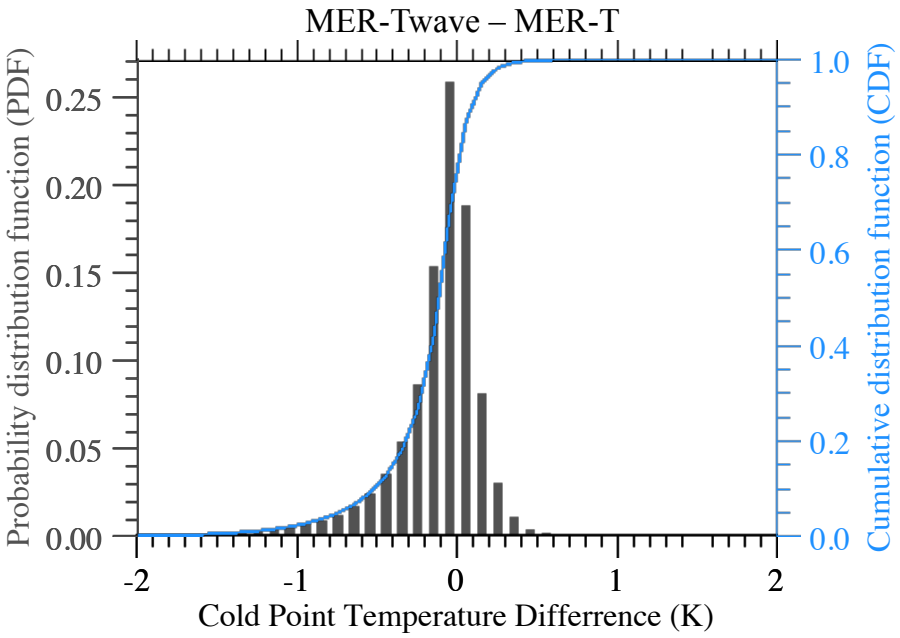

Fig. 3. Cold-Point temperature differences between MERRA adjusted by waves and MERRA (MER-Twave – MER-T) during 2007-2013. The PDF in black is plotted on left-y axis and CDF in blue on right-y axis.

570

571

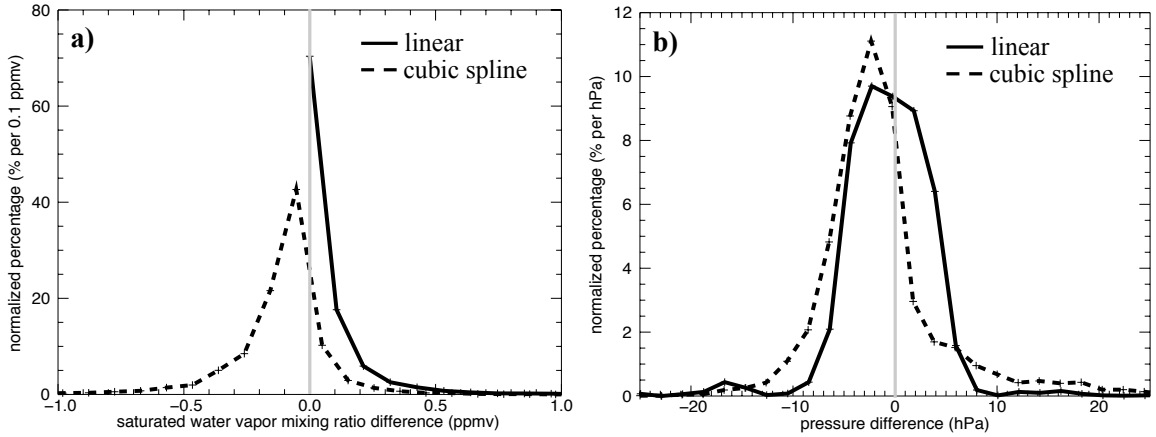

Fig. 4. PDFs of the differences between linear or cubic spline interpolations to the actual value form the GPS temperature profiles. (a) Minimum saturation mixing ratio of the profile (units are percent per 0.1 ppmv); (b) pressure of the saturation mixing ratio minimum (units are percent per hPa). The plus signs in each line mark the bin intervals.

572

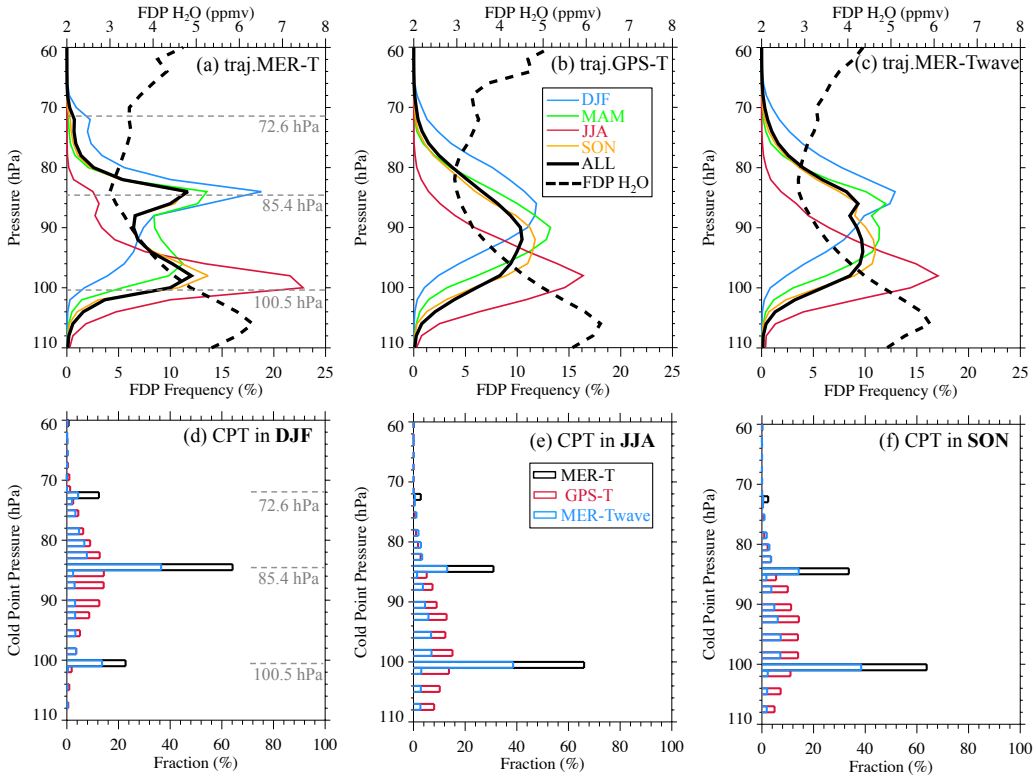

Fig. 5. Seasonal FDP vertical distributions (in %, solid lines, lower x axis) and FDP saturation mixing ratio (FDP-H_2O, i.e., the stratosphere entry level H_2O, ppmv, dashed lines, upper x axis) from trajectory simulations using (a) MERRA temperatures, (b) GPS temperatures, and MERRA temperatures adjusted by waves (c), compared to the cold point tropopause statistics during (d) DJF, (e) JJA, and (f) SON. The FDP frequency is normalized by total FDP events, so each solid curve adds up to 100%. The MERRA model levels at 100.5 and 85.4 hPa are marked panel a.

573

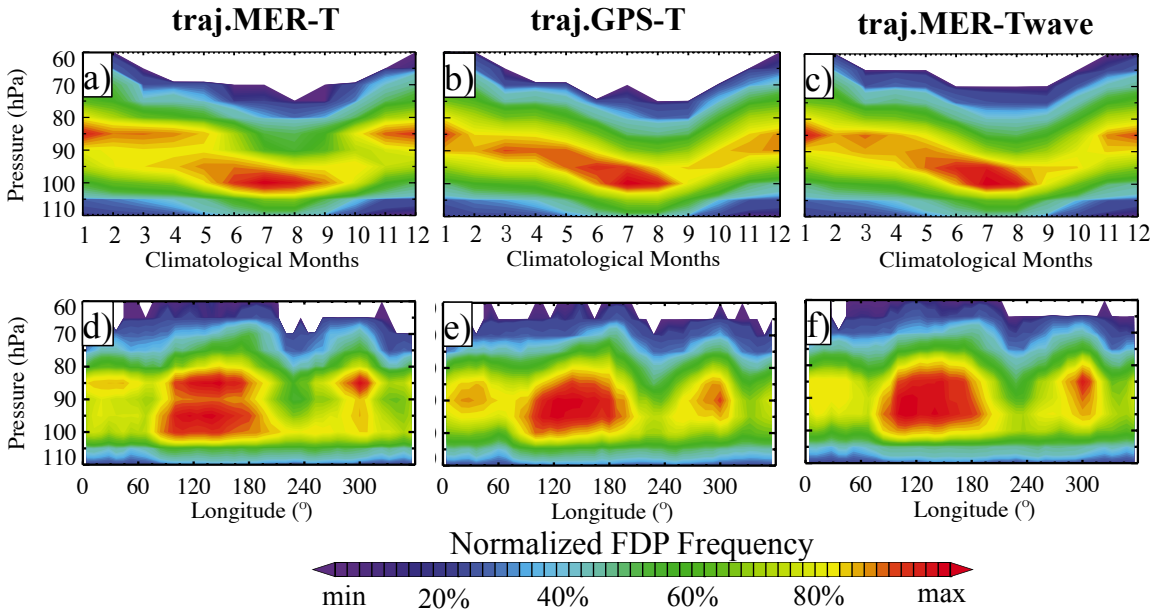

Fig. 6. Vertical distributions of normalized FDP events in time-evolutional (a-c) views among trajectory simulations by using a) MERRA temperature (*traj.MER-T*), b) GPS RO temperature (*traj.GPS-T*), and c) MERRA temperature adjusted by waves (*traj.MER-Twave*). The longitudinal variations of FDP are highlighted in panel d-f to emphasize the FDP discontinuity in *traj.MER-T*. All panels are plotted in their own range and color-coded at the same percentiles (i.e., 0, 20%, 40%, …, 100%) to compare the patterns.

574

575

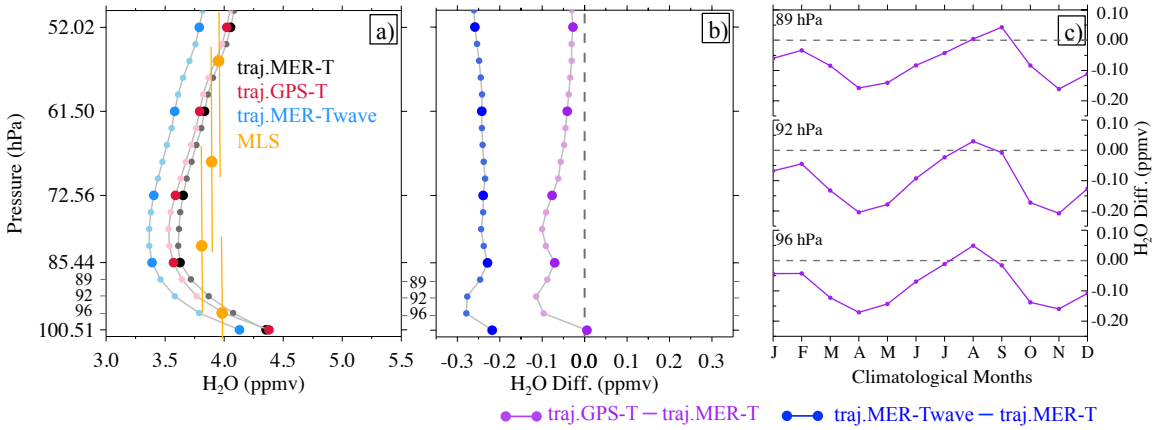

Fig. 7. (a) Trajectory predicted H_2O compared with MLS observations (the vertical bars in orange indicate the MLS vertical resolutions at each of the MLS retrieval pressure levels); (b) trajectory H_2O differences induced by waves (blue) and by using GPS temperatures (purple); (c) annual differences at 96, 92, and 89 hPa. All values are averaged over the deep tropics (18°S–18°N) in 2007-2013, with larger dots marking the MERRA model levels and small dots marking the MERRA in-between levels – those are the levels that the cold-point tropopause could have been found but not available in current MERRA vertical resolution.

576

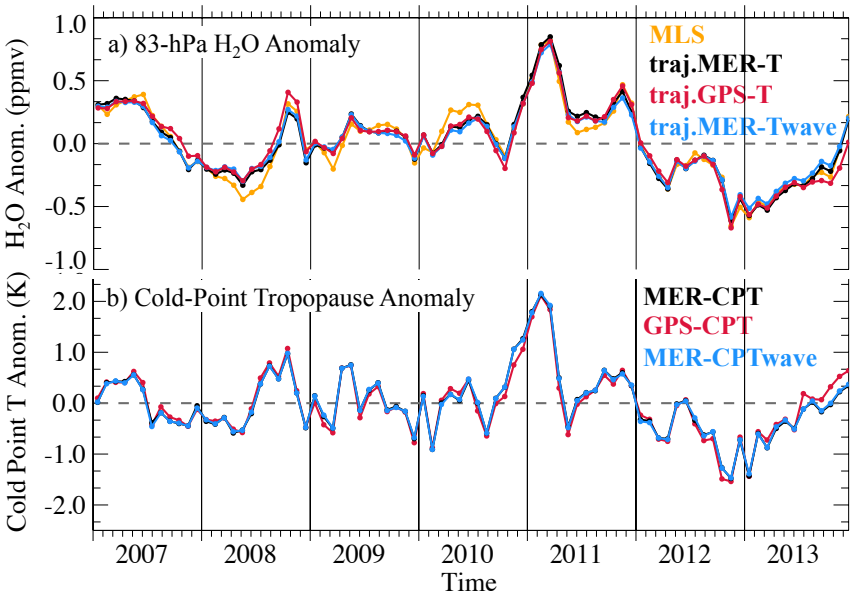

Fig. 8. (a) Trajectory simulated H_2O anomalies compared with the MLS observations; and (b) cold-point temperature anomalies from three temperature datasets. All time series are averaged over the deep tropics (18^oN-18^oS). All trajectory results in panel a are weighted by the MLS averaging kernels for far comparison.

577